Antibacterial metal ion release from diamond-like carbon modified surfaces for novel multifunctional implant materials

Sascha Buchegger, Caroline Vogel, Rudolf Herrmann, Bernd Stritzker, Achim Wixforth, Christoph Westerhausen

Angaben zur Veröffentlichung / Publication details:

Buchegger, Sascha, Caroline Vogel, Rudolf Herrmann, Bernd Stritzker, Achim Wixforth, and Christoph Westerhausen. 2016. "Antibacterial metal ion release from diamond-like carbon modified surfaces for novel multifunctional implant materials." *Journal of Materials Research* 31 (17): 2571–77. https://doi.org/10.1557/jmr.2016.275.

Antibacterial metal ion release from diamond-like carbon modified surfaces for novel multifunctional implant materials

Sascha Buchegger, Caroline Vogel, Rudolf Herrmann, Bernd Stritzker, Achim Wixforth and Christoph Westerhausen

***Abstract*—The aim of this study was the synthesis of hard and low-abrasive novel implant materials with built-in time-dependent antibacterial properties, which can be tailored by a well-defined time-dependent and finite release of metal ions. We were able to synthesize such smart implant surfaces employing ECR (electron cyclotron resonance)-plasma on typical titanium implant material by transforming a polymer film into diamond-like carbon (DLC) which contains metal nanoparticles as reservoirs for controlled metal ion release. We found that the amount of released antibacterial metal ions is a biexponential function of time with a high release rate during the first few hours followed by a decreased ion release rate within the following days. To describe our experimental findings, we developed a kinetic model assuming that both nanoparticles near the surface and nanoparticles in the DLC bulk contribute to the total amount of ions released with different time constants.**

Keywords — biomedical; ion-beam processing; sol-gel

Affiliations
Sascha Buchegger, Caroline Vogel, Rudolf Herrmann, Bernd Stritzker
Chair for Experimental Physics 1, University of Augsburg, Universitätsstr. 1, 86159 Augsburg, Germany

Achim Wixforth, and Christoph Westerhausen
1. Chair for Experimental Physics 1, University of Augsburg, Universitätsstr. 1, 86159 Augsburg, Germany
2. Nanosystems Initiative Munich, Schellingstraße 4, 80799 Munich, Germany
3. Augsburg Center for Innovative Technologies (ACIT), 86159 Augsburg, Germany

1. Introduction

Despite many efforts in the field of clinical hygiene research, healthcare-associated infections are still a serious problem and frequently lead to revision surgeries. According to recent studies, joint replacements require still almost 7 % revision, and infections due to surfaces harboring bacteria, such as gram positive *staphylococci* [1], are amongst the most prominent post-operative incidents [1, 2]. As the aging population and hence the need for implants grows in Western countries, this serious problem will presumably even increase in the future. Novel and innovative scientific approaches thus, amongst others, aim towards an appropriate biofunctionalization of implant surfaces. Especially for articulated joint surfaces, the most important demands are biocompatibility, time-dependent antibacterial activity and profound corrosion- as well as wear resistance. In terms of antibacterial performance, modern implant surfaces should ideally provide a tailored antibacterial behavior with a large initial antibacterial activity during the first 24 h after implantation. This way, implant-associated infections could be avoided and the implant surface would be protected against bacterial adhesion and subsequent biofilm formation [3, 4]. The initial fast action should be followed by a continuously decreasing antibacterial activity within the subsequent few days.

To create such intelligent implant surfaces with optimized hardness, wear and corrosion resistance and at the same time exhibiting the desired antibacterial properties, we employed an energetic ion treatment of a functionalized polymeric surface layer. This polymer layer is containing metallic nanoparticles (NP) and then is transformed into a very hard and wear resistant DLC layer, still containing the metal NPs.

The transformation method of our choice is the Plasma Immersion Ion Implantation (PIII), a surface modification process that improves the wear resistance by forming a very hard layer on the material surface [5]. During the PIII process, the polymeric surface is surrounded by non-condensing plasma whereupon a pulsed bias (5-20 kV) is applied to an electrode coupled to the polymer surface to be modified. Due to their acceleration in the plasma, the impinging ions are implanted below the surface leading to hydrogen effusion. Subsequent rebonding of the displaced atoms then results in a well-defined DLC layer, having the desired low friction coefficient and high density and perfect hardness. DLC has been proven in the past to represent an outstanding coating material and has been in the focus of research for medical materials for several years [5–8]. By our transformation process of functional polymer layers containing metal NP, we combine these outstanding properties with additional antibacterial ones.

In terms of antibacterial applications, Ag, Cu and ZnO nanoparticles (NPs), of order 100 nm in size, are receiving more and more attention. Several mechanisms have been reported for the antibacterial activity of metal NPs. Their antibacterial activity is related to the generation and release of ions from the particle surface into the biological system, where smaller particles result in faster ion release than larger ones [9–11]. The antibacterial effectiveness of NPs is assumed to result from a combination of their small size, fast dissolution in a given volume and high surface-to-volume ratio providing close interactions with microbial membranes [12]. Especially silver NPs have been proven to ensure high antimicrobial efficacy while showing low cytotoxicity[1], but antimicrobial activity has also been demonstrated for nano-sized Cu particles [12]. Because of its selective toxicity mainly targeting prokaryotic systems, also ZnO NPs can be used to reduce microbe attachment and viability on medical surfaces [13, 14]. According to [15], $AgNO_3$, $CuCl_2$ and $ZnCl_2$ metal salts display a concentration-dependent cytotoxicity with inhibitory concentration (IC_{50}) values of 3.23 mg/L, 5.08 mg/L and 4.58 mg/L, respectively. Hence, the cytotoxic effect of the NPs mentioned above seems to decrease following the sequence Ag>Cu>ZnO. Various biomedical applications using antibacterial NPs have emerged on the market over the last years: Prominent examples include venous catheters coated with Ag NPs or Cu and ZnO NPs within dental materials [16–18]. Regarding medical DLC applications, DLC coated stents were also investigated [6]. Moreover, DLC was found to be a versatile coating material for endoprosthesis and dental implants and other applications [19]. While there are publications on the copper ion release kinetics of plasma-polymer coatings[20, 21], there are no publications on quantitative metal ion release from DLC. Some reports, however, on doping DLC with Ag, Cu and V to create antibacterial properties[19, 22, 23], exist in the literature. These publications report in detail about the material properties and the biological effect *in vitro* but not on quantitative release kinetics. However, there is still a lack of promising implant materials being wear resistant and antimicrobial due to tailorable Ag, Cu or Zn release at the same time. Here, we demonstrate a novel approach to synthesize antibacterial implant materials by the combination of a dip-coating polymer deposition process and subsequent DLC transformation employing our PIII technique. We thus obtain materials fulfilling the above mentioned essential requirements for articulated joint implants like mechanical stability, biocompatibility, and time-dependent antibacterial metal ion release. These modified DLC surfaces are supposed to have low abrasive properties. In this study, we report for the first time on the ion release kinetics of Ag, Cu and Zn from DLC. Knowledge about these kinetics is crucial for tailoring desired ion release from medical implants.

2. Materials and methods

2.1. Materials

Cylindrical titanium alloy (Ti6Al4V) samples (Ø: 10 mm, thickness: 2 mm), provided by Aesculap AG Tuttlingen, were used as substrate material. The sample surfaces exhibit a roughness of R_q= 5 µm, which is due to a corundum blasting step. For the coating, we prepared a colloidal poly(vinylpyrrolidone) (PVP) solution, containing the Ag, Cu or ZnO NPs. Ag NPs were directly formed in the polymer solution while the Cu or ZnO NPs were synthesized in a separate step beforehand.

To prepare the Ag containing polymer dip-coating solution, stock solutions of poly(vinylpyrrolidone) (PVP, MW 55000, Sigma-Aldrich, 66.7 g/l) in ethanol, silver nitrate ($AgNO_3$, 17.0 g/l) in ethanol and benzoin (10.6 g/l) in acetone were prepared. Here benzoin acts as photoinitiator. These stock solutions were mixed in the volume ratio 1:3:3 ('Ag 1'), 1:0.6:0.6 ('Ag 1/5') and 1:0.3:0.3 ('Ag 1/10') starting with 75 ml of PVP solution. After the complete dissolution of all reactants, the solution was UV-irradiated with a mercury lamp (36 W) from a distance of 25 cm for 12 hours leading to a light-induced reduction of the $AgNO_3$ and subsequent formation of Ag NPs. These NP dispersions were used for the dip-coating process without further treatment for the samples Ag 1/5 and Ag 1/10, whereas the total volume of the highest Ag concentration was reduced to 150 ml by evaporation.

The ZnO NPs were prepared separately from the PVP solution as described elsewhere [24, 25] and stored in dry ethanol (Emsure quality, Merck). For the according coating, we prepared a dispersion containing 500 mg of ZnO NPs and 5.0 g of PVP in 145 ml dry ethanol.

Similarly, the Cu NPs were synthesized employing a modification of a standard protocol [26]. Here, a copper salt ($CuCl_2$ ≥98%, Merck, 0.4 g), PVP (6.48 g) and poly(ethylene glycol) (PEG, MW 8000, Sigma Aldrich, 8.52 g), were dissolved under a slow N_2 stream in 120 ml deionized water and heated to 70°C (oil bath temperature). Aqueous NH_3 solution (25%, 3.0 ml) was added and the mixture was stirred for 45 min. Hydrazine sulfate (≥99%, Sigma-Aldrich, 2.22 g) was added and stirred for another 100 min at 70°C, followed by 16 h stirring at room temperature. The NPs were finally separated by centrifugation (6700g, 15 min), re-dispersed in 70 ml of deionized water, centrifuged again and re-dispersed in 70 ml of ethanol (last step repeated). The particles were stored in ethanol (16 ml). For the Cu NP containing samples, dispersions containing 500 mg of NPs and 5.0 g of PVP in 145 ml of ethanol were used.

2.2. Sample preparation and characterization

To create a well-defined polymeric film on top of our implant Ti6Al4V samples, we used a dip coating technique. The samples were mounted on a steel plate using adhesive carbon tape and then dipped into the colloidal polymer solution containing either the Ag, Cu or ZnO NPs. The film thickness was adjusted by a variation of the dipping velocity (here 0.75 mm/s) and the viscosity of

the solution. After dipping, the complete sample was covered with the polymer film except for the backside which stuck to the holder.

To obtain a polymer-to-DLC surface transformation, the coated samples were dried in air and then treated by a PIII process. The samples were immersed into a microwave plasma (f=2.45 GHz) consisting of Ne (47.7 %), Ar (32.7 %) and CH_4 (19.6 %) for t=73 min at $p=3\cdot10^{-3}$ mbar, while a pulsed bias U=-20 kV was applied to the sample holder at a frequency of 200 Hz and a pulse length of 5 µs, leading to a DLC layer of 40-50 nm thickness. To further elucidate the sample preparation procedure, we schematically presented it in FIG. 1. To characterize the final functional DLC layers, Raman spectroscopy (sp3 content, see FIG. 2) as well as nano-hardness measurements were performed. We used an ASMEC UNAT nanoindenter(Asmec GmbH, Rossendorf, Germany) in QCSM mode. Here, an additional force vibration is modulated on top of the force ramp which allows to measure depth-dependent hardness. We applied a maximum force of 0,6mN using a diamond Berkovich tip.

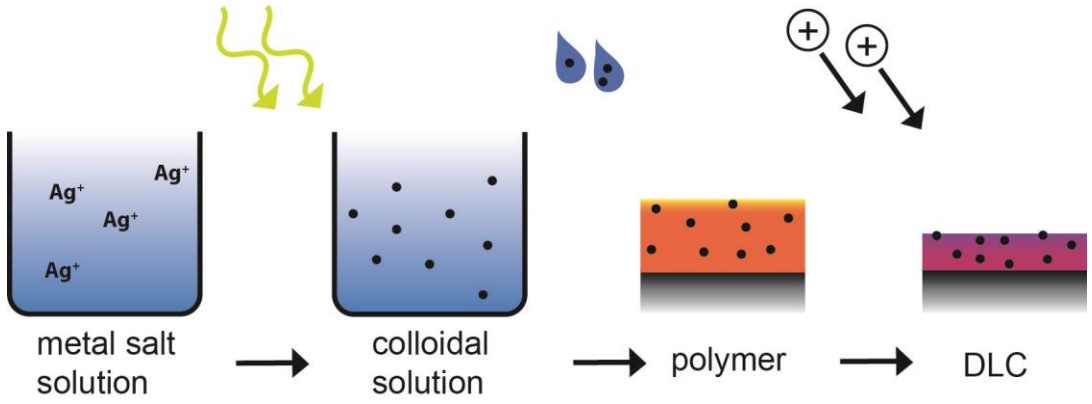

FIG. 1. Sample preparation procedure. The figure schematically shows the dip-coating process used to cover the samples' surface by a polymer film for Ag containing samples, reproduced from [27]. Accelerated ions were implanted into the surface creating a modified DLC layer with a thickness of tens of nanometers. The first two steps were omitted for Cu and ZnO samples.

2.3. Nanoparticle characterization

In order to obtain information about the Ag, Cu and ZnO NPs, their size and morphology, we employed Transmission Electron Microscopy (TEM) investigations with a Jeol JEM 2100 F instrument (see FIG. 3). Here, small droplets of the colloidal solutions were deposited and dried on standard carbon-coated copper grids (Plano GmbH).

2.4. Metal ion release measurements

To investigate the metal ion release for the functionalized DLC samples, two identical samples from each batch (Ag, Cu, ZnO) were embedded in paraffin wax, leaving a total surface area of 1.57 cm^2 exposed. To prevent ion release from the sample edges, they were covered by a metal protective paint (AkzoNobel). Afterwards, all samples were immersed into 10 ml calf serum solution (Biochrom GmbH, protein concentration of 30 g/l, containing EDTA as stabilizer and Amphotericin B from Calbiochem to prohibit fungal infection) and kept in a standard incubator at 37 °C. After defined periods of time, the calf serum solution was completely exchanged and the total concentrations were measured employing Inductively Coupled Plasma-Optical Emission Spectroscopy (Varian ICP-OES) equipped with an autosampler. The presented data in figure 4 represent the mean values from three independent samples.

3. Results and discussion

3.1. DLC characterization

To characterize the hybridization type in the DLC-layer, we performed Raman spectroscopy measurements (see FIG. 2). The so-called D and G peaks in the spectra were fitted by Lorentzians and the intensity ratio of both modes, I(D)/I(G), was calculated. This ratio as well as the shift of the G-Peak were compared with literature values published by Robertson et al. [28] to determine the sp^3 fraction of the carbon atoms. All Raman spectra resulted in sp^3 fractions of approximately 35% in the material, which is a typical value for a-C:H networks. Also, nano-hardness testing was done to prove the success of the DLC-transformation. Hardness measurements resulted in typical DLC hardness values of about 14 GPa for the samples produced. Due to the low thickness of the DLC layer compared to the indentation depth, however, some influence from the substrate might inflict the measurements. However, in presently ongoing studies, we also measured the hardness of nominally identical but thicker coatings (multi-layer DLC, produced by repeated dip-coating and ion implantation process, to be published elsewhere) with thicknesses $d > 500$ nm. For those samples, the indentation depth was below 10% of the film thickness. The hardness of such multi-layer DLC samples is expected to be lower than a single layer DLC coating as the range in the repeated ion bombardment process is greater than the layer thickness. This leads to partial graphitization of the lower layer, which in turn leads to an overall hardness decrease. Nevertheless, hardness values of 12 GPa, typical for a-C:H networks, were measured. As the focus of this work, however, lies on the tailored metal ion release from DLC layers, we did not intensively study wear resistance. Nevertheless, preliminary studies

using a standardized tribological setup, where a DLC coated sphere was moved with a defined load on a flat DLC surface in calf serum solution, showed no significant debris according to ISO 17853 after two million cycles. Using a steel tip, it is not possible to scratch the coating by hand. Thus, we feel safe to claim typical DLC properties for the samples used here.

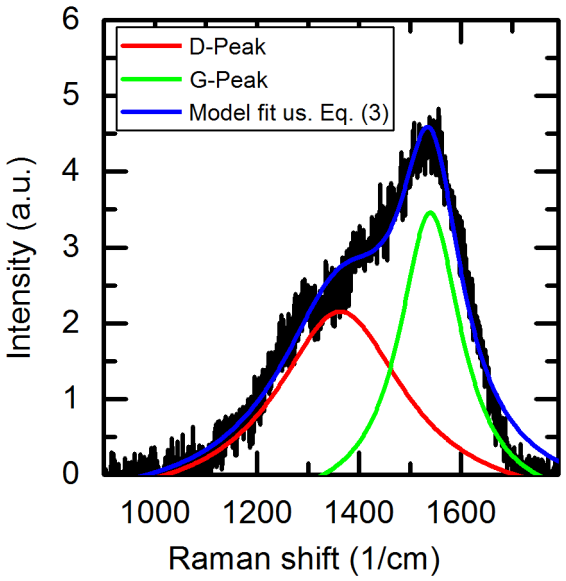

FIG. 2. Raman spectrum of the DLC layer. The green and red lines show the Lorentzian of D and G peaks, respectively. The cumulative fit is represented by the blue line. The I(D)/I(G) ratio is a measure for the sp^3 fraction of the carbon atoms.

3.2. Nanoparticle characterization

Morphology and size of the synthesized nanoparticles were characterized using transmission electron microscopy. The Cu NPs formed large agglomerates (FIG. 3 (a)) consisting of nearly spherical nanoparticles as depicted in FIG. 3 (b). The ZnO NPs are less spherical and tend to form small aggregates (FIG. 3 (d)) whereas the spherical Ag NPs were more dispersed (FIG. 3 (c-d)) but show a wider size distribution than the Cu and ZnO NPs.

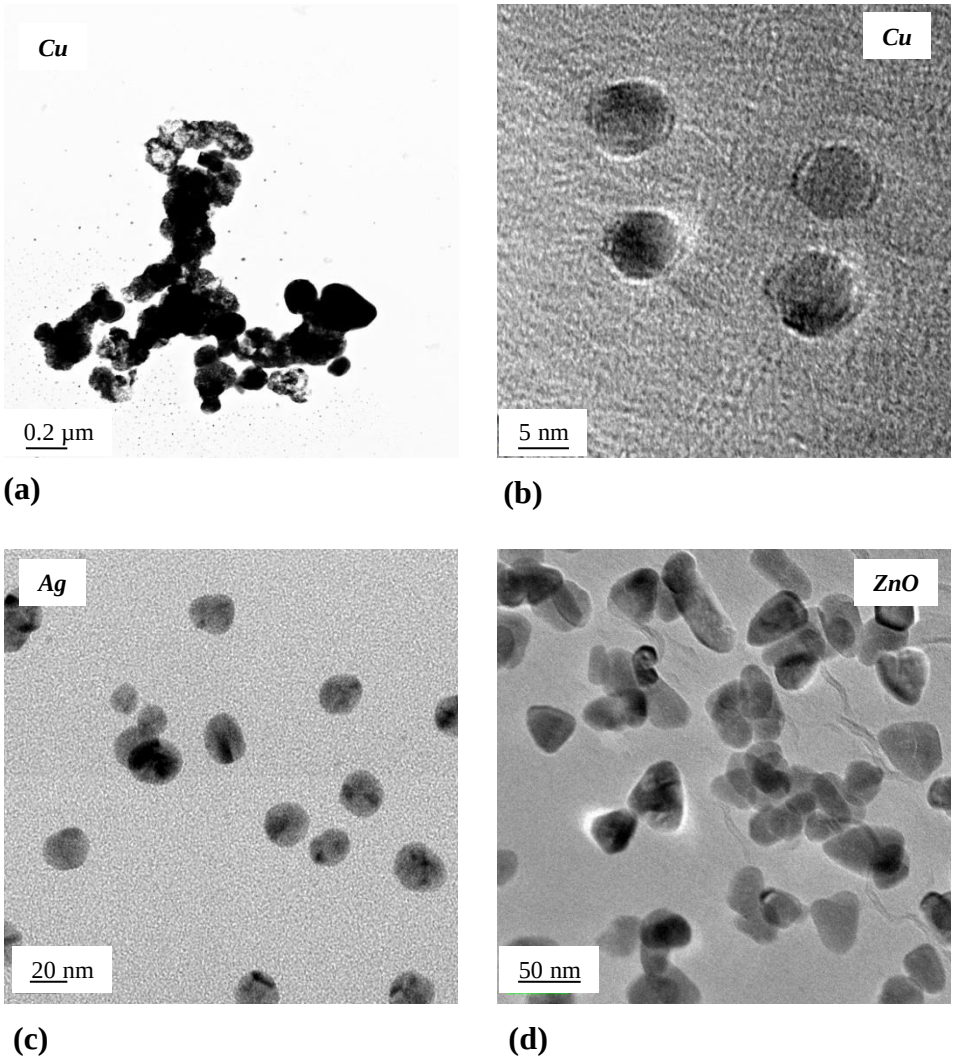

FIG. 3. Microscopical investigation of NPs. TEM (Transmission Electron Microscopy) micrographs of (a-b) Cu NPs, (c) Ag NPs and (d) ZnO NPs dispersed in polymer solution. Cu NPs formed large agglomerates (a) consisting of nano-sized nearly spherical particles as depicted in micrograph (b). Ag NPs and ZnO NPs (c-d) show a greater dispersion while ZnO NPs forms smaller aggregates (d) and have a less spherical shape than Ag NPs and Cu NPs.

3.3. Metal ion release

As depicted in figure 4, all samples tested kept releasing metal ions into the calf serum solution for several days. The absolute amount of ions released from the DLC layer differed strongly for different metals, with highest ion release for Zn, followed by Cu and Ag.

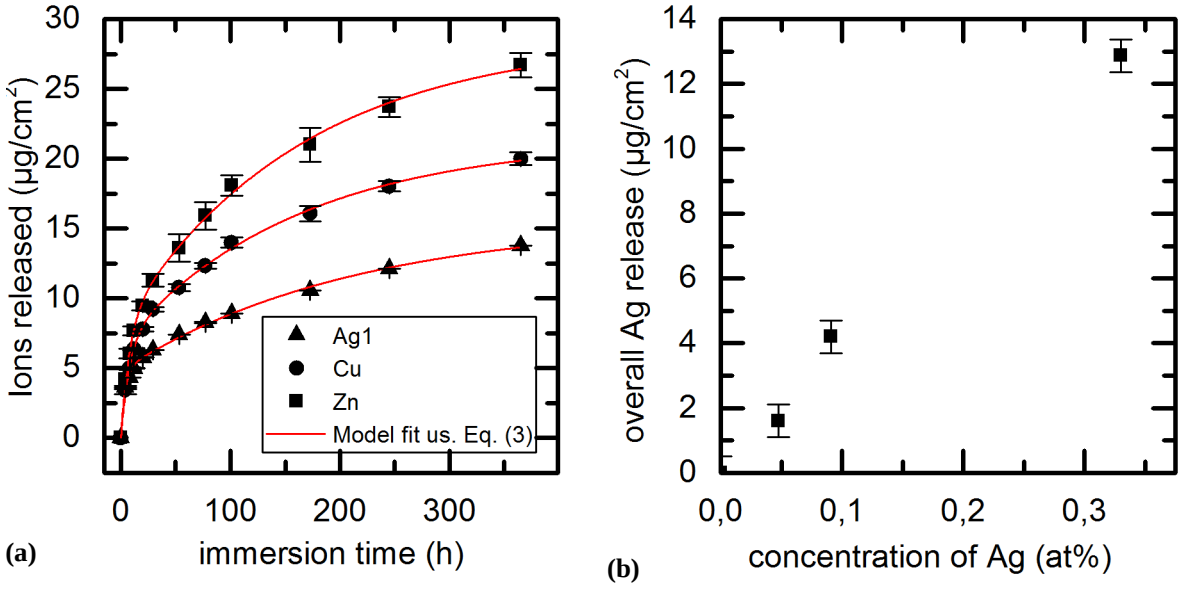

FIG. 4. Metal ion release. (a) Cumulative ion release from DLC films into calf serum as a function of immersion time. The red lines are model fits (eq. 3). In most cases, error bars were smaller than respective data points and (b) linear relationship between Ag concentration in the DLC sample and cumulative Ag ion release.

Moreover, the ion release was found to be a time-dependent two-stage process, with fast increase during the first days followed by a decrease within the next few days. We attribute this behavior to a purely geometrical effect: NPs at or partially sticking out of the surface and NPs completely "buried" in the DLC contribute differently to the ion release. Whereas NPs in contact to the aqueous solution immediately release free ions, metal ions from those in the bulk need to diffuse to the surface before entering the fluid. Hence, the ion release during the first decay time t_1 predominantly depends on the fast oxidation by oxygen (of Ag and Cu) and the hydration of the ions, as depicted in FIG. 5.

The kinetics of nanoparticle dissolution was considered before [29–31] by looking at the oxidation reaction stoichiometry of Ag NPs being (partially) exposed to the aqueous environment (scenario 1 in FIG. 5):

$$2\,Ag_{(s)} + \tfrac{1}{2}\,O_{2(aq)} + 2H^{+}_{(aq)} \leftrightarrow 2Ag^{+}_{(aq)} + H_2O \qquad (1)$$

Using an Arrhenius ansatz, the Ag^+ release rate γ_{Ag^+} was derived as [29]:

$$\gamma_{Ag^+} \sim r^2 T^{1/2} \exp\left(\frac{-E_a}{k_B T}\right) [\text{Ag NPs}][O_2]^{0.5}[H^+]^2 \qquad (2)$$

Here, r is the radius of Ag NPs, k_B is the Boltzmann constant, E_a is the activation energy, and [Ag NPs], $[O_2]$ and $[H^+]$ are respective molar concentrations. Further adaptations of Eq. (1) lead to the total amount of released ions which was used before to describe the experimental data with a and $[Ag]_0$ as fitting parameters.

$$[Ag^+]_{released} = [Ag]_0 [1 - \exp(-at)] \qquad (2)$$

However, the microscopic origin and mechanism leading to the second time constant in the release measurements is not yet clear, to date. Theoretically, this mechanism could be diffusion of either bare or hydrated metal ions through the DLC. In the latter case, water could either diffuse into the DLC or be formed by hydrogen from the DLC and oxygen diffusing into the DLC. To the knowledge of the authors, however, there are no reports on these mechanisms for amorphous DLC, yet. In any case, the fact that ions are released and detected at two different time scales indicates that there *must* be one escape mechanism available which seems not to be present for dry samples, which remain stable for weeks after preparation. Figure 5 illustrates the assumed ion release process described above. Independent of the actual transport mechanism, a diffusive behavior and hence a kinetic of the same type as eq. 2 is obvious. Consequently, the total amount A of released metal ions was modeled as a combination of ion release contributing from the surface (*, scenario 1 in FIG. 5) and from the bulk (**, scenario 2 in FIG. 5)

$$A(t) = \underbrace{A_1\left[1 - \exp\left(-\frac{t}{t_1}\right)\right]}_{(*)} + \underbrace{A_2\left[1 - \exp\left(-\frac{t}{t_2}\right)\right]}_{(**)} \qquad (3)$$

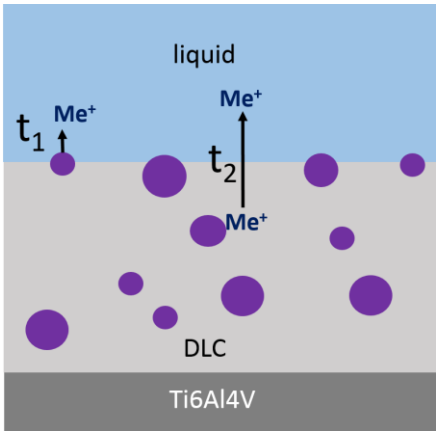

FIG. 5. Assumed ion release process. Schematic representation of the proposed ion release process with ion release from NPs at the surface during the initial decay time t_1 and diffusion of ions towards the DLC surface occurring during the second decay time t_2.

Eq. (3) was used to fit the experimental results with A_1, A_2, t_1 and t_2 being fitting parameters using the non-linear Levenberg Marquardt algorithm (see FIG. 4). The release in the first few days is dominated by the amount A_1 released from or near the surface. A summary of all fitting parameters is shown in Table 1. The fitted values of A_1, t_1 and t_2 for Cu and Zn are quite similar, whereas the values of A_2 were slightly different, but still comparable in the order of magnitude. This finding suggests that the release and subsequent transport mechanism of Cu and Zn ions through the DLC is rather similar. This might be due to the similar ion radii of Cu and Zn and charge of the released ions (Cu^{2+} and Zn^{2+} vs. Ag^{+}). The differences in total ion release $A_{tot}= A_1+A_2$ of Zn^{2+} and Cu^{2+} ions can be explained by deviations of the precursor film thickness and used NP concentration. The mass ratio of embedded ZnO and Cu determined by RBS measurements (data not shown) displays qualitatively the ratio of $A_{tot,Zn}$:$A_{tot,Cu}$.

TABLE I. Calculated fitting parameters. Parameters A_1, A_2, t_1 and t_2, of Ag NPs, Cu NPs or ZnO NPs containing DLC samples calculated from the developed model fit.

	'Ag 1'	**'Cu'**	**'Zn'**
A_1 **[µg/cm²]**	4.21	6.82	8.04
A_2 **[µg/cm²]**	10.24	14.59	20.67
t_1 **[h]**	3.85	7.70	7.72
t_2 **[h]**	196.02	162.76	165.35

Figure 4 (b) depicts a nearly linear ion release as a function of Ag concentration for three initial concentrations in the colloidal solution ('Ag 1'→'Ag 1/5'→'Ag 1/10'), Hence, we deduce from our data that a tailorable Ag ion release seems to be adjustable through the proper choice of initial $AgNO_3$ concentration.

4. Conclusion

The presented study was undertaken to synthesize novel implant materials fulfilling the basic desired requirements for artificial joint applications including appropriate wear resistance and time-dependent antibacterial activity. As a matter of fact, all fabricated samples show DLC characteristics in terms of hardness as well as sp^3 content and all samples in fact released the desired Ag, Cu and Zn ions from the DLC surface layer thus providing antibacterial functionality. From our findings, we deduct a model to further fine tune various ion release kinetic aspects by a variation of the ratio of near-surface and 'buried' NPs.

To give a rough estimate for the relevance of an antimicrobial effect, we here exemplarily consider the Ag ion release within 24 h for an 'Ag 1' sample: If we assume the knee joint's surface area to be 50 cm^2, our model reveals an amount of 0.3 mg Ag ions released into the knee joint. For an average volume of a male adult's knee joint of V=103.6 ml [32], a global Ag concentration of 2.9 mg/L in the knee is obtained. This value is higher than the minimum inhibitory concentration against *S. aureus* (2.5 mg/L) but lower than IC_{50} (3.23 mg/L) for the inhibition of fibroblasts' cell metabolism [33]. This ensures the potential of the material for an effective antibacterial treatment, especially as we may assume that locally the Ag concentration might be even higher.

In summary, we have demonstrated a method for tailored ion release from Ag NPs containing DLC surfaces exhibiting a linear relationship between the initial $AgNO_3$ concentration in the sample and the amount of released Ag ions. This relationship in fact allows for the precise adaption of the desired antibacterial activity of wear and corrosion resistant DLC coatings on medical implants. Our experimental findings and results have the evident potential to provide a platform for the design and development of various novel wear resist and antibacterial implant materials, being highly relevant for future clinical applications.

Disclosures

The authors have no financial conflicts of interest.

Acknowledgments

The authors like to thank the “Deutsche Forschungsgemeinschaft (DFG)” for the financial support of this research work in form of the “Erkenntnistransferprojekt Antibakterielle und abriebarme Beschichtung von Gleitflächen in orthopädischen Implantaten” and Aesculap AG Tuttlingen for providing required materials. CW likes to acknowledge funding by Nanosystems Initiative Munich (NIM).

References

1 L. Pauksch, M. Rohnke, R. Schnettler and K. S. Lips, Silver nanoparticles do not alter human osteoclastogenesis but induce cellular uptake. *Toxicol. Reports*. **1**,900–908 (2014).

2 K. Grandfield, Bone, implants, and their interfaces. *Phys. Today*. **68**,40–45 (2015).

3 D. R. Monteiro, L. F. Gorup, A. S. Takamiya, A. C. Ruvollo-Filho, E. R. de Camargo and D. B. Barbosa, The growing importance of materials that prevent microbial adhesion: antimicrobial effect of medical devices containing silver. *Int. J. Antimicrob. Agents*. **34**,103–110 (2009).

4 C. P. McCoy, R. A. Craig, S. M. McGlinchey, L. Carson, D. S. Jones and S. P. Gorman, Surface localisation of photosensitisers on intraocular lens biomaterials for prevention of infectious endophthalmitis and retinal protection. *Biomaterials*. **33**,7952–7958 (2012).

5 M. T. Mohammed, Z. A. Khan and A. N. Siddiquee, Surface Modifications of Titanium Materials for developing Corrosion Behavior in Human Body Environment: A Review. *Procedia Mater. Sci.* **6**,1610–1618 (2014).

6 K. Gutensohn, C. Beythien, J. Bau, T. Fenner, P. Grewe, R. Koester, K. Padmanaban and P. Kuehnl, In Vitro Analyses of Diamond-like Carbon Coated Stents. *Thromb. Res.* **99**,577–585 (2000).

7 F. R. Marciano, D. A. Lima-Oliveira, N. S. Da-Silva, A. V. Diniz, E. J. Corat and V. J. Trava-Airoldi, Antibacterial activity of DLC films containing TiO2 nanoparticles. *J. Colloid Interface Sci.* **340**,87–92 (2009).

8 F. Schwarz and B. Stritzker, Plasma immersion ion implantation of polymers and silver–polymer nano composites. *Surf. Coatings Technol.* **204**,1875–1879 (2010).

9 E. A. Elkhawass, M. E. Mohallal and M. F. M. Soliman, Acute toxicity of different sizes of silver nanoparticles intraperitonally injected in balb / c mice using two toxicological methods. *Int J Pharm Pharm Sci*. **7**,94–99 (2015).

10 C. Damm and H. Münstedt, Kinetic aspects of the silver ion release from antimicrobial polyamide/silver nanocomposites. *Appl. Phys. A*. **91**,479–486 (2008).

11 H. Ma, P. L. Williams and S. A. Diamond, Ecotoxicity of manufactured ZnO nanoparticles – A review. *Environ. Pollut.* **172**,76–85 (2013).

12 H. L. Karlsson, P. Cronholm, Y. Hedberg, M. Tornberg, L. De Battice, S. Svedhem and I. O. Wallinder, Cell membrane damage and protein interaction induced by copper containing nanoparticles—Importance of the metal release process. *Toxicology*. **313**,59–69 (2013).

13 W. Salem, D. R. Leitner, F. G. Zingl, G. Schratter, R. Prassl, W. Goessler, J. Reidl and S. Schild, Antibacterial activity of silver and zinc nanoparticles against Vibrio cholerae and enterotoxic Escherichia coli. *Int. J. Med. Microbiol.* **305**,85–95 (2015).

14 H. Ma, P. L. Williams and S. a. Diamond, Ecotoxicity of manufactured ZnO nanoparticles - A review. *Environ. Pollut.* **172**,76–85 (2013).

15 E. N. Sowa-Söhle, A. Schwenke, P. Wagener, A. Weiss, H. Wiegel, C. L. Sajti, A. Haverich, S. Barcikowski and A. Loos, Antimicrobial efficacy, cytotoxicity, and ion release of mixed metal (Ag, Cu, Zn, Mg) nanoparticle polymer composite implant material. *BioNanoMaterials*. **14** (2013), doi:10.1515/bnm-2013-0012.

[16] K. Chaloupka, Y. Malam and A. M. Seifalian, Nanosilver as a new generation of nanoproduct in biomedical applications. *Trends Biotechnol.* **28**,580–588 (2010).

[17] R. P. Allaker, The Use of Nanoparticles to Control Oral Biofilm Formation. *J. Dent. Res.* **89**,1175–1186 (2010).

[18] B. Aydin Sevinç and L. Hanley, Antibacterial activity of dental composites containing zinc oxide nanoparticles. *J. Biomed. Mater. Res. Part B Appl. Biomater.* **94B**,22–31 (2010).

[19] F. P. Schwarz, I. Hauser-Gerspach, T. Waltimo and B. Stritzker, Antibacterial properties of silver containing diamond like carbon coatings produced by ion induced polymer densification. *Surf. Coatings Technol.* **205**,4850–4854 (2011).

[20] W. Zhang, Y. Zhang, J. Ji, Q. Yan, A. Huang and P. K. Chu, Antimicrobial polyethylene with controlled copper release. *J. Biomed. Mater. Res. Part A.* **83A**,838–844 (2007).

[21] P. K. Chu, Applications of plasma-based technology to microelectronics and biomedical engineering. *Surf. Coatings Technol.* **203**,2793–2798 (2009).

[22] G. Francz, A. Schröder and R. Hauert, Surface analysis and bioreactions of Ti- and V-containing a-C: H. *Surf. Interface Anal.* **28**,3–7 (1999).

[23] R. Hauert, A review of modified DLC coatings for biological applications. *Diam. Relat. Mater.* **12**,583–589 (2003).

[24] M. M. Demir, R. Munoz-Espi, I. Lieberwirth and G. Wegner, Precipitation of monodisperse ZnO nanocrystals via acid-catalyzed esterification of zinc acetate. *J. Mater. Chem.* **16**,2940 (2006).

[25] R. Herrmann, F. J. García-García and A. Reller, Rapid degradation of zinc oxide nanoparticles by phosphate ions. *Beilstein J. Nanotechnol.* **5**,2007–2015 (2014).

[26] P. P. Chowdury, A. H. Shaik and J. Chakraborty, Preparation of stable sub 10 nm copper nanopowders redispersible in polar and non-polar solvents. *Coll. Surf. A.* **466**,189–196 (2015).

[27] F. P. Schwarz, thesis, Dissertation, Augsburg (2010).

[28] J. Robertson, Diamond-like amorphous carbon. *Mater. Sci. Eng. R Reports.* **37**,129–281 (2002).

[29] W. Zhang, Y. Yao, N. Sullivan and Y. S. Chen, Modeling the Primary Size Effects of Citrate-Coated Silver Nanoparticles on Their Ion Release Kinetics. *Environ. Sci. Technol.* **45**,4422–4428 (2011).

[30] E. A. Meulenkamp, Size Dependence of the Dissolution of ZnO Nanoparticles. *J. Phys. Chem. B.* **102**,7764–7769 (1998).

[31] C.-M. Ho, S. K.-W. Yau, C.-N. Lok, M.-H. So and C.-M. Che, Oxidative Dissolution of Silver Nanoparticles by Biologically Relevant Oxidants: A Kinetic and Mechanistic Study. *Chem. - An Asian J.* **5**,285–293 (2010).

[32] T. Visuri and O. Kiviluoto, Arthroscopic Volume of the Knee Joint in Young Male Adults. *Scand. J. Rheumatol.* **15**,251–254 (1986).

[33] S. Chernousova and M. Epple, Silver as Antibacterial Agent: Ion, Nanoparticle, and Metal. *Angew. Chemie Int. Ed.* **52**,1636–1653 (2013).